Cerebrovascular systems with concomitant pathologies:A computational hemodynamics study

Marcelo A. Castro[1]
CONICET. Universidad Tecnológica Nacional, Facultad Regional Buenos Aires
Grupo de Investigación y Desarrollo en Bioingeniería
Medrano 951, Ciudad Autónoma de Buenos Aires, CP 1179, Argentina

E-mail: marcelo.a.castro@gmail.com

Nora L. Peloc
Universidad Favaloro, Facultad de Ingeniería, Ciencias Exactas y Naturales
Solís 453, Ciudad Autónoma de Buenos Aires, CP 1078, Argentina

Juan R. Cebral
George Mason University. College of Sciences
4400 University Drive, Fairfax, VA, 22030, USA

Abstract. Although unusual, cerebral aneurysms may coexist with a proximal artery stenosis. In that small percent of patients, such coexistence poses a challenge for interventional neuroradiologists and neurosurgeons to make the best treatment decision. According to previous studies, the incidence of cerebral aneurysms in patients with internal carotid artery stenosis is not greater than 5%, where the aneurysm is usually incidentally detected, being 2% for aneurysms and stenoses in the same cerebral circulation. Those cases pose a difficult management decision for the physician. Case reports showed patients who died due to aneurysm rupture months after endarterectomy but before aneurysm clipping, while others did not show any change in the aneurysm after plaque removal, having optimum outcome after aneurysm coiling. The aim of this study is to investigate the intraaneurysmal hemodynamic changes before and after treatment of stenotic plaque. Idealized models were constructed with different stenotic grade, distance and relative position to the aneurysm. Digital removal of the stenotic plaque was performed in the reconstructed model of a patient with both pathologies. Computational fluid dynamic simulations were performed using a finite element method approach. Blood velocity field and hemodynamic forces were recorded and analyzed. Changes in the flow patterns and wall shear stress values and distributions were observed in both ideal and image-based models. Detailed investigation of wall shear stress distributions in patients with both pathologies is required to make the best management decision.

[1] To whom any correspondence should be addressed.

Content from this work may be used under the terms of the Creative Commons Attribution 3.0 licence. Any further distribution of this work must maintain attribution to the author(s) and the title of the work, journal citation and DOI.
Published under licence by IOP Publishing Ltd

Introduction

Intracranial aneurysms and artery stenosis are vascular diseases with different characteristics. According to previous studies, the incidence of cerebral aneurysms in patients with internal carotid artery stenosis is 2.3-4.9 %, where the aneurysm is usually incidentally detected [1-3]. A retrospective study of 853 patients with stenosis in the carotid bifurcation showed that 46 patients (5.4%) had a cerebral aneurysm, while only 2% had the aneurysm in the same arterial circulation [4]. A case report showed that a patient with a stenosis in the carotid artery and an asymptomatic unruptured aneurysm (5.0x10.0 mm) in the same artery at the posterior communicating artery bifurcation underwent a successful endarterectomy. The patient died after a subarachnoid hemorrhage five months after the intervention. Autopsy revealed that the aneurysm had growth up to 14.0x10.0 mm. before rupture [5]. Another case report describes the treatment option for a patient with similar characteristics. A stenosis in the carotid artery was located proximal to an unruptured aneurysm (14.0x8.0 mm.) at the ophthalmic artery bifurcation. A stent was successfully deployed to remove the stenosis. A few months after the intervention, no change was observed in the aneurysm size and the aneurysm was treated with a coil embolization procedure [1]. The treatment option has risk and benefits that must be studied by the physician in a patient-specific basis. Removing the stenosis may result in aneurysm rupture due to flow changes. In addition, a brain surgery to treat the aneurysm may cause a stroke because of flow reduction. Simultaneous interventions were also reported [6]. In this work we analyze the hemodynamic characteristics at cerebral aneurysms before and after the virtual removal of a proximal stenotic plaque. Idealized models were created to investigate changes of velocity and wall shear stress at the aneurysm after intervention, depending on stenosis grade and relative position to the aneurysm. A patient-specific model with a proximal stenosis was included. The plaque was digitally removed using a Laplacian filter and the aneurysm hemodynamic characteristics were compared.

Materials and methods

1.1. Idealized models

Three patients with cerebral aneurysms in the AComA were selected from our data base. In order to minimize the dependency of the results on the reconstruction of the normal vascular models, all images presenting an extension of the disease towards further regions beyond the aneurysm neck were rejected for this study. Bilateral rotational scans were obtained to visualize both avenues of flow into the anterior communicating artery (AcomA) aneurysm using a Philips Integris System [8]. Images were obtained during a 180° rotation and imaging at 15 frames per second for 8 seconds. The 120 projection images were reconstructed into a 3D dataset of 128 128 128 voxels covering a field of view of 54.02 mm on a dedicated Philips Integris workstation. The voxel resolution was therefore 0.422 mm. These data were exported into a PC for mathematic vascular modelling using a previously presented methodology [19,20,10]. Models were edited and aneurysms were virtually removed.

1.2. Patients and images

Rotational cerebral angiography images are the preferred modality for reconstructing vascular models harboring aneurysms due to their highest spatial resolution and contrast. For the selected patient, a rotational scan was obtained to visualize the pathologic vasculature. An 8-second acquisition consisted in 120 projections obtained during a 180° rotation, which were reconstructed into a 3D dataset of 128^3 voxels covering a field of view of 54.02 mm on a dedicated workstation. The voxel resolution was therefore 0.422 mm. These data were exported into a PC for mathematic vascular modeling using a previously presented methodology [8,9,10,11]. The imaging protocol was approved by the institutional review board and informed consent was obtained from the subject.

1.3. Vascular modeling

Finite element blood flow numerical simulations were performed for all models under the same flow conditions. Blood was modelled as an incompressible Newtonian fluid with attenuation 1.0 g/cm^3 and

viscosity 0.04 Poise. The governing equations were the unsteady Navier-Stokes equations in 3D [15]. Vessel walls were assumed rigid, and no slip boundary conditions were applied at the walls. Pulsatile flow conditions derived from phase-contrast magnetic resonance measurement in a healthy subject were imposed at the inlet of the models. Flow waveforms were scaled with the inlet area in order to achieve a mean WSS of 15 dyn/cm^2 at the inflow boundary of each model. This choice is consistent with studies relating vessel area and flow rates in internal carotid and vertebral arteries [16], as well as with the principle of minimal work expressed by Murray's law [17]. Fully developed pulsatile velocity profiles were prescribed with the use of the Womersley solution [18,19]. Assuming that all distal vascular beds have similar total resistance to flow, traction-free boundary conditions with the same pressure level were applied at outlet boundaries. The Navier-Stokes equations were numerically integrated by using a fully implicit finite element formulation [9]. We computed 2 cardiac cycles using 100 time-steps per cycle, and all of the reported results correspond to the second cardiac cycle.

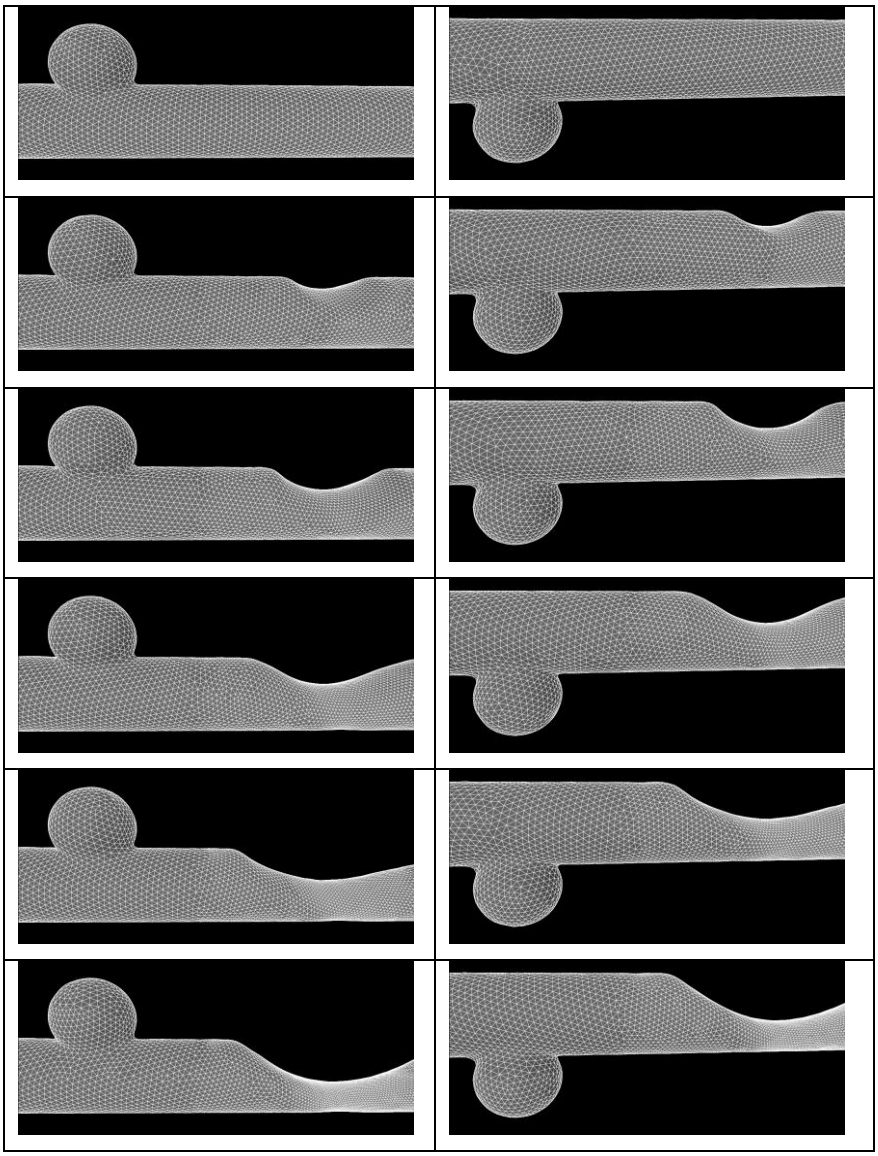


Figure 1. This picture shows all idealized models for the minimum distance between the aneurysm and the stenosis (1.60 cm). Left column: aneurysm ipsilateral to the stenosis. Right column: aneurysm contralateral to the stenosis. Each row corresponds to a different grade of stenosis. From top to bottom: 0, 20, 40, 55, 65 and 75.

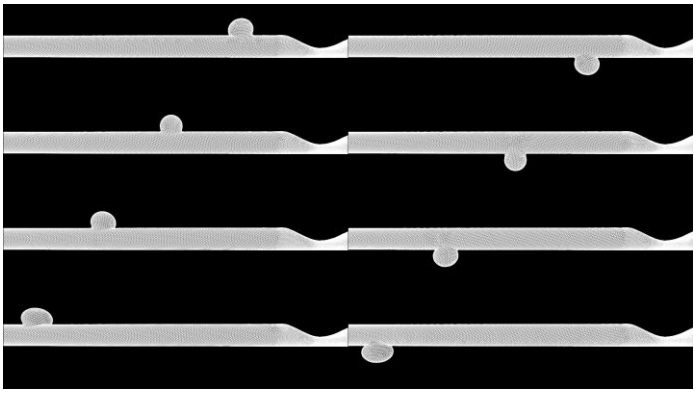


Figure 2. This picture shows all idealized models for the 75-degree stenosis. Left panel: aneurysm ipsilateral to the stenosis. Right panel: aneurysm contralateral to the stenosis. Each row corresponds to a different distance between the aneurysm and the stenosis. From top to bottom: 1.60 cm, 3.20 cm, 4.80 cm and 6.40 cm.

1.4. Data analysis

Maps of WSS magnitude were created to visualize the distribution of shear forces on the aneurysm wall and the vessel. Magnitude of the velocity and vector field was computed at cutplane containing the vessel axis, the aneurysm dome and the maximum narrowing of the artery.

Results

In order to investigate how changes in the flow pattern due to the stenosis grade may affect the intraaneurysmal hemodynamics, magnitude of the velocity and vector field at a cutplane containing the vessel axis, the aneurysm dome and the maximum narrowing at the systolic peak were displayed (Figures 3a and 3b). Wall shear stress maps were constructed to study how its distribution depends on the stenosis grade (Figures 4a and 4b). The same flow rate wave form was applied to all models. Severe stenoses were not included in this study, therefore no inflow correction was imposed at the inlet of the model after virtual intervention with respect to the original diseased arteries.

Eccentric stenoses generate a recirculation at distal regions adjacent and ipsilateral to the stenosis along with a main jet narrowing and shift towards the opposite side. That produces lower velocity and wall shear stress in the post stenotic vortex adjacent to the stenosis, and higher values in the opposite side. The extension of the recirculation zone is minimal for low stenosis grades but significantly increases with the severity of the disease. That region is associated with lower wall shear stress values compared to the vessel without stenotic plaque. For higher stenosis grades, the recirculation pattern results in higher velocity and wall shear stress values over a larger area. For distal aneurysms ipsilateral to the high degree stenoses, the vortex may reach the aneurysm depending on the stenosis grade and the distance between the aneurysm and the stenosis. Under this condition, the part of the neck closer to the aneurysm witnesses high velocities (see Figures 3a) resulting in higher wall shear stress values (see Figure 4a).

It is also observed that the higher the stenosis grade, the higher the jet narrowing and the higher the wall shear stress values right downstream the vessel narrowing. However, because of jet concentration, those values become lower than the average in the normal vessel when the jet heads towards the vessel axis (see Figures 4a and 4b). Those values increase again when the jet develops towards its ideal Womersley profile in a cylindrical vessel.

For aneurysms contralateral to the stenosis the intraaneurysmal flow pattern is not affected by the recirculation. However, for high stenosis grades the jet is deflected towards the aneurysm resulting in higher WSS values in the distal part of the neck (see Figure 4b). The part of the vessel under flow recirculation experiments higher WSS values for mild stenoses compared to a normal vessel. But now that effect takes place diametrically opposite to the aneurysm, which is contralateral to the stenosis.

The typical lateral aneurysm in a straight vessel exhibits a higher WSS region in the distal part of the neck. However, when a proximal aneurysm is present changes in the WSS values both in the

distal and proximal part of the aneurysm neck appear. Therefore, if the stenosis is removed, forces over the aneurysm neck will change depending on the WSS distributions before and after the intervention. For aneurysms ipsilateral to the stenosis, the WSS at the distal part of the neck is less affected by the plaque. However, for higher grades, that region starts to feel the disturbance caused by the recirculation vortex resulting in lower WSS values. For the distance between the aneurysm and the stenosis and the stenosis grades considered here, the distal part of the neck remains outside that vortex. On the other hand, the proximal part is under lower velocities and WSS values when the vortex reaches that region, which is observed for 55% and 65% degree stenosis, and suddenly increases for higher grades (e.g. 75% degree stenosis) because the vortex region is large enough to enter the aneurysm resulting in higher velocities upstream in the proximal part of the neck and WSS values even higher than those observed when no stenosis is present (see Figure 5). Note that for all other configurations the WSS in the aneurysm is lower with than without stenosis because the stenosis produces a concentration of the flow with higher velocities and flow rate confined to a main jet far from the walls in the post-stenotic region.

It is also observed that for higher stenosis grades the WSS at the distal part of the neck is much lower in aneurysms ipsilateral to the stenosis than for contralateral ones. That is due to the fact that ipsilateral aneurysms are affected by the recirculation vortex for higher grades.

Considering that an endarterectomy would affect the intra-aneurysmal hemodynamics, the pre- and post-intervention WSS maximum values in the aneurysm at the systolic peak were compared for the 65% degree stenosis case for both ipsilateral and contralateral configurations. It was observed that for ipsilateral configurations the maximum WSS, which occurs at the distal region of the neck, would increase from 39.0 dyn/cm^2 to 65.3 dyn/cm^2 (67.6%), while for contralateral configurations it would increase from 51.5 dyn/cm^2 to 65.3 dyn/cm^2 (26.7%). Note that 65.3 dyn/cm^2 corresponds to the WSS value at the systolic peak in the distal region of the aneurysm neck when no proximal stenosis is present. That observation shows that hemodynamics of lateral aneurysms contralateral to a proximal eccentric artery stenosis is considerably less affected compared to ipsilateral configurations.

For the patient-specific model, the same inflow rate waveform was used, which was scaled in order to impose a mean wall shear stress of 15 dyn/cm^2 at the internal carotid artery [16,17]. The inflow waveform had been previously acquired from a normal subject using phase-contrast magnetic resonance angiography imaging [8,11]. Three regions were selected to compare the WSS values before and after the intervention, ordered according to the distance to the stenosis: I) proximal part of the first lobulation neck close to the stenosis; II) peak value at the neck of the second lobulation; III) peak value at the dome of the second lobulation. High WSS values at region (I) dropped from 720 dyn/cm^2 to 270 dyn/cm^2. The region (II), which is located downstream, exhibits almost no difference in peak WSS: 235 dyn/cm^2 (before) compared to 219 dyn/cm^2 (after). That is due to the fact that although the jet is less concentrated, it impacts straight on the neck of the second lobulation. Finally, for region (III) the jet is much less concentrated after the intervention resulting in a low WSS of 20 dyn/cm^2 at the dome after the intervention compared to 150 dyn/cm^2 before the intervention (see Figure 6). In this patient-specific case it can be observed that some high WSS regions reduce their values after intervention while others remain approximately the same.

Although it is not expected flow alterations after the removal of a 65% grade stenotic plaque, a virtual experiment was performed by decreasing the pre-intervention flow in 30% according to reported data for higher stenosis grades. In this experiment it was observed a lower WSS in the dome before the intervention, because of a lower flow. However, it is still higher that that after the plaque removal, due to jet dissipation. On the other hand, lower flow before the intervention results in lower WSS values at the neck of the first lobulations. Those values significantly increase after the intervention because of a higher flow. This virtual experiment suggest that removing a stenotic plaque may relocate regions of high and low WSS, which may eventually change the biological response of endothelial cells to flow forces (see Figure 7).

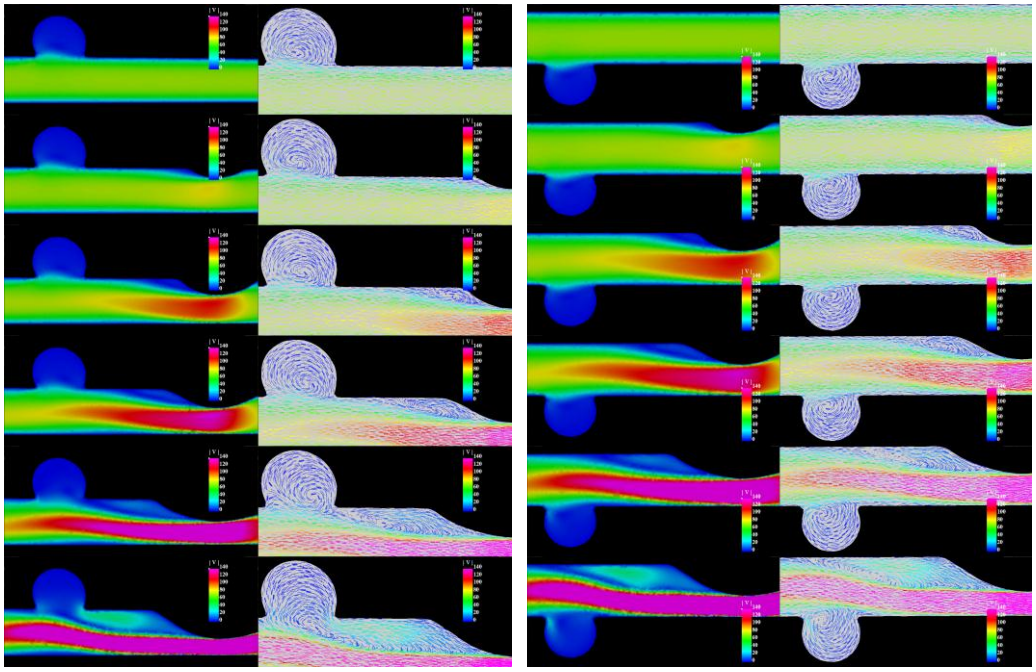


Figure 3**.** a) LEFT PANEL: ipsilateral cases ; b) RIGHT PANEL: contralateral cases. Magnitude of the velocity (left columns) and vector field (right columns) at the systolic peak at a cutplane containing the vessel axis, the aneurysm dome and the maximum narrowing, for aneurysms ipsilateral to the stenosis. Each row corresponds to a different grade of stenosis. From top to bottom: 0, 20, 40, 55, 65 and 75. Color maps range between the minimum velocity value of 0 cm/sec (blue) and >140 cm/sec (magenta).

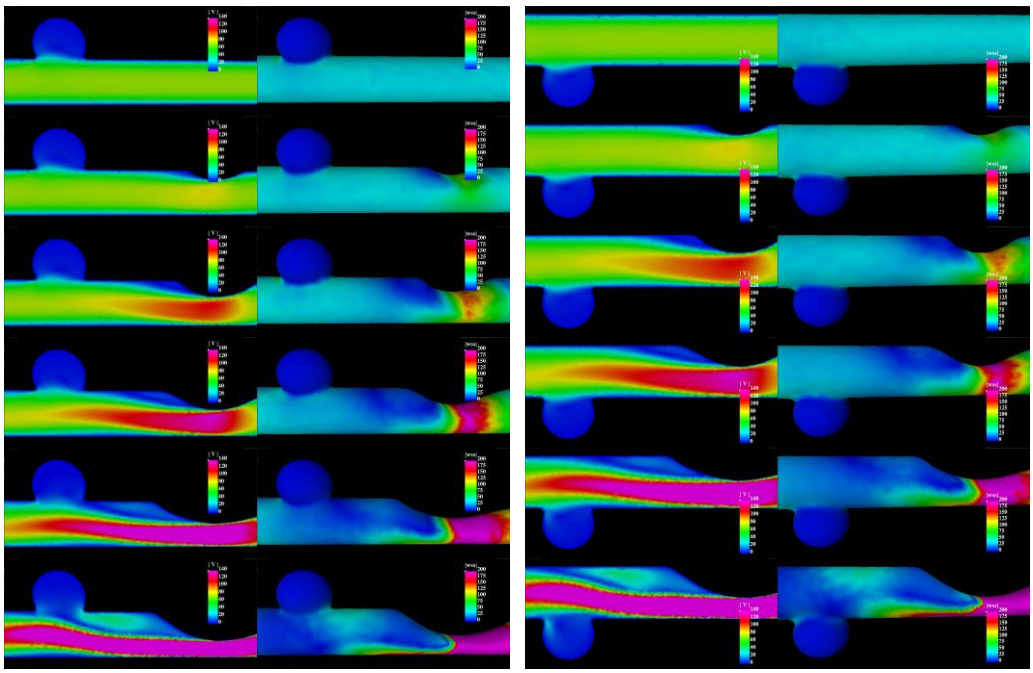


Figure 4**.** a) LEFT PANEL: ipsilateral cases ; b) RIGHT PANEL: contralateral cases. Magnitude of the velocity (left columns) and wall shear stress distribution (right columns) at the systolic peak at a cutplane for aneurysms ipsilateral to the stenosis. Each row corresponds to a different grade of stenosis. From top to bottom: 0, 20, 40, 55, 65 and 75. Color maps range for the velocity range between 0 cm/sec (blue) and >140 cm/sec (magenta), while for the wall shear stress range between 0 dyn/cm^2 and >200 dyn/cm^2.

Discussion

In this paper we applied a previous developed methodology for patient-specific image-based computational hemodynamics studies of vascular cerebral networks harboring intracranial aneurysms [4,10,14,19] to study the intra-aneurysmal hemodynamics in patients having a cerebral aneurysm distal to a artery stenosis in the same circulation. Patients with concomitant carotid artery stenosis and unruptured intracranial aneurysms pose a difficult management decision for the physicians. Case reports showed patients who died due to aneurysm rupture months after endarterectomy but before aneurysm clipping, while others did not show any change in the aneurysm after plaque removal, having optimum outcome after aneurysm coiling [1,5].

The aim of this preliminary work is to investigate the main characteristics of the intra-aneurysmal hemodynamics affected by a proximal artery stenosis, and the expected changes after a plaque removal. For that purpose, a set of forty eight idealized CFD models of lateral aneurysms located at different positions from a proximal eccentric stenosis was constructed. Vector velocity field and wall shear stress distributions were examined for different distances between the aneurysm and the stenosis, for aneurysms both ipsilateral and contralateral to the stenosis, and for six different stenosis grades (low and mild). It could be observed that the recirculation distal to the stenosis may significantly affect the intraaneurysmal hemodynamics of ipsilateral aneurysms increasing the wall shear stress values in the proximal part of the neck. On the other hand, contralateral aneurysms may experience an increment of the wall shear stress in the distal part of the neck due to the deflection and narrowing of the main jet in the post-stenotic region. Those effects are relevant in the vascular zone closer to the aneurysm. However, for high stenosis grades, the recirculation extends further downstream resulting in higher wall shear stress gradients. Comparison between the intraaneurysmal hemodynamics before and after a plaque removal may help to estimate the changes in the hemodynamic quantities and their impact on the risk of rupture.

Flow alterations after the removal of a 65% grade stenotic plaque are not expected. However, a virtual experiment was performed by reducing the pre-intervention flow in 30% according to reported data for higher stenosis grades. It was observed a lower WSS in the dome before the intervention, because of a lower flow. However, it is still higher that that after the plaque removal, due to jet dissipation. On the other hand, lower flow before the intervention results in lower WSS values at the neck of the first lobulations. Those values significantly increase after the intervention because of a higher flow. This virtual experiment suggest that removing a stenotic plaque may relocate regions of high and low WSS, which may eventually change the biological response of endothelial cells to flow forces.

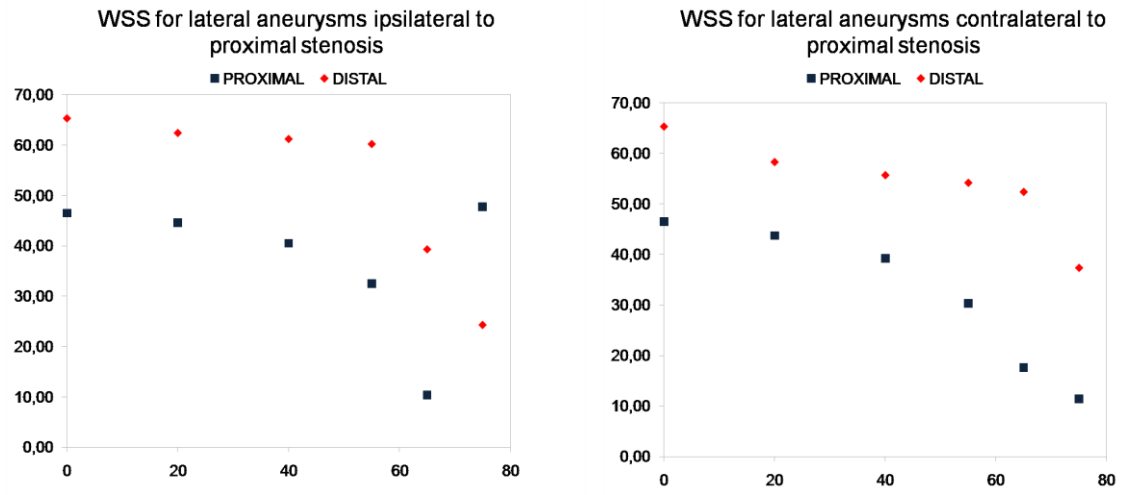


Figure 5. Magnitude of the absolute value of the wall shear stress distribution at the systolic for aneurysm ipsilateral (left column) and contralateral (right column) to the stenosis at both the proximal and distal part of the neck.

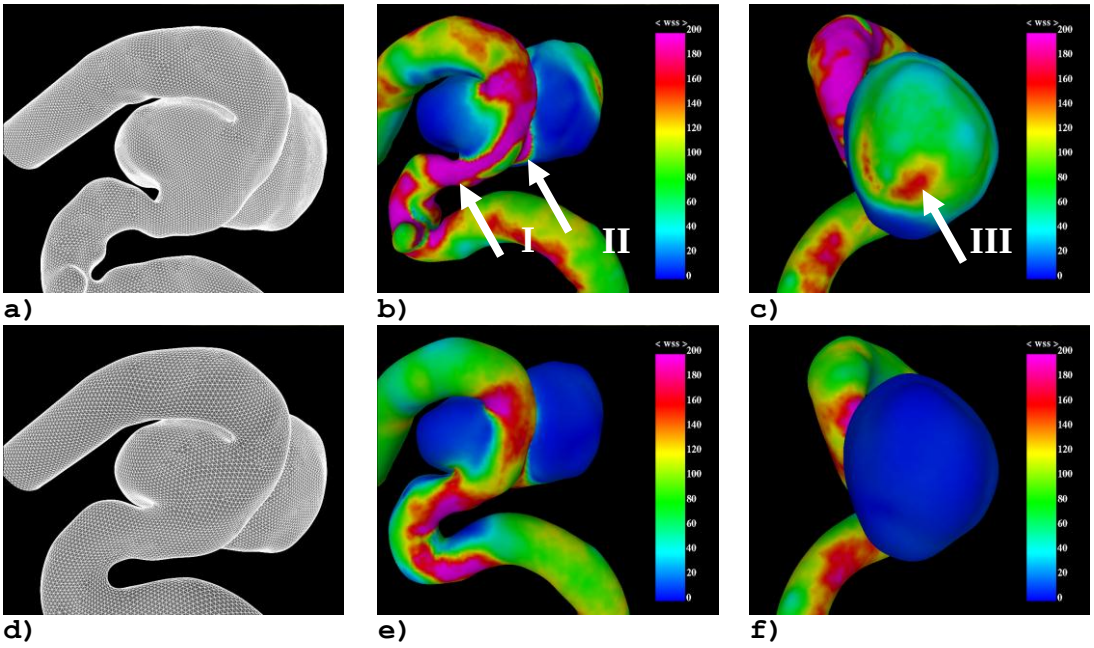


Figure 6. Vascular model before (a) and after (d) removal of proximal stenosis. Wall shear stress distributions before (b and c) and after (e and f) virtual intervention.

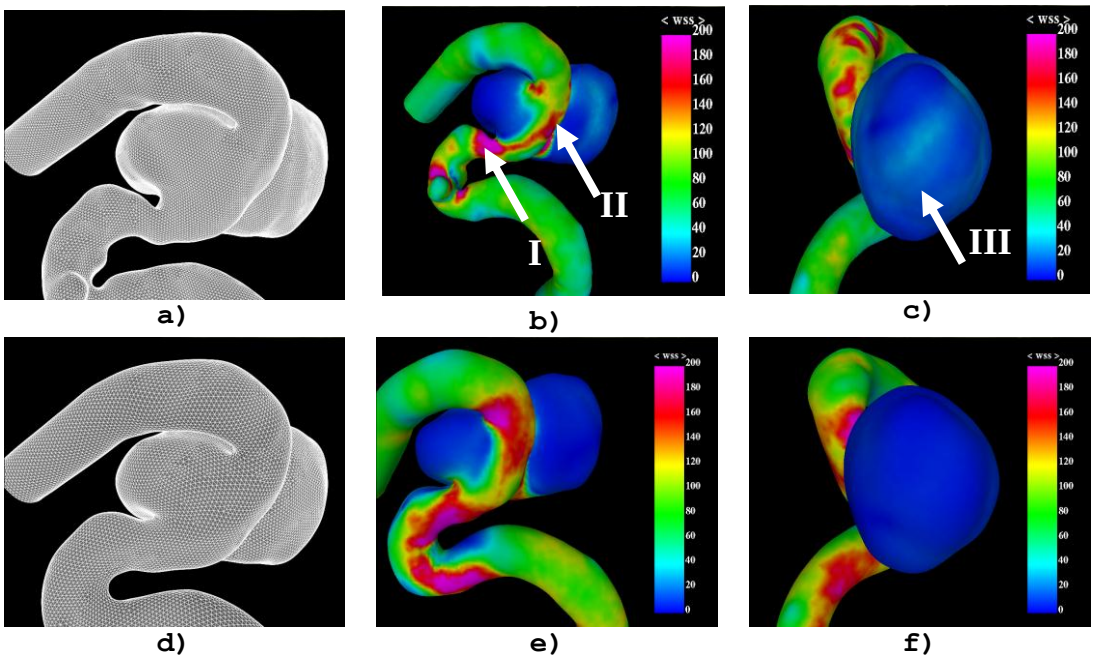


Figure 7. Vascular model before (a) and after (d) removal of proximal stenosis, considering lower flow rate before the intervention due to the stenotic plaque. Wall shear stress distributions before (b and c) and after (e and f) virtual intervention.

For severe stenoses, which are beyond the scope of this work, transition to turbulence begins to play an important role. Varghese et al. investigated in detail the hemodynamic characteristics through a 75-degree stenosis using an idealized model of an eccentric stenosis using direct numerical simulations [20]. However, those models did not include distal aneurysms. In a previous work, Varghese et al. compared the prediction of post-stenotic velocity field and wall shear stress as well as shear stress peak at the throat of the stenosis in a pulsatile regime through an idealized stenotic vessel (75% axisymmetric stenosis) using four different turbulent models implemented in a popular commercial CFD code, with respect to two previous experiments that described stenotic flows [21].

They found discrepancies between the different turbulent models. The low Reynolds number *k-ω* turbulent model was closer to the experimental results. All of them predicted low wall shear stress values distal to the stenosis as a consequence of high jet concentration, which is in agreement with our results.

Patel et al. reviewed several turbulence models for low Reynolds number flows [22]. They found that many of the models lacked generality and were restricted by the choice of empirical constants, being the Chien model the one that performed better compared to the others. All *k-ε* models use wall functions to obtain near-wall results. Since accurate estimation of wall shear stress in one of the main goals in the problem under study, such models may not be the wisest choice. From that point of view, *k-ω* models may be more suitable for stenotic flows. However, the transitional nature of this kind of flows suggest the use of direct numerical simulations to resolve the flow, although that will be a complex undertaking in realistic diseased 3D vessels under pulsatile flow conditions [23].

Additionally, we selected a case from our data base corresponding to a patient with a cerebral aneurysm right distal to an artery stenosis. The diseased artery exhibited a two-lobe aneurysm, impacting the main jet into the dome of one of them. The aneurysm formed right downstream of the stenosis and the narrowed jet produced a small impaction zone with high wall shear stress values. The stenosis was virtually removed by means of the use of Laplacian filters and the intraaneurysmal hemodynamics was compared before and after the intervention. Wall shear stress at that dome reduced about one order of magnitude after the plaque was removed.

The methodology has some limitations. The study only included low and mild stenoses. Severe stenosis would require higher resolution models to correctly depict transition to turbulence and also to consider flow correction after the intervention. Although the removal of a high degree stenotic plaque may significantly affect the intraaneurysmal hemodynamics, the post-intervention flow may return to its higher normal value, resulting in higher forces exerted on the aneurismal wall, and increasing the risk of rupture. Vascular models with aneurysms distal to a severe stenosis will be studied in detail. Another limitation is that hemodynamic characteristics observed in ideal cases may not necessarily be representative of real cases. For that purpose, a patient-specific case was also studied. Although the correct vascular geometry reconstruction results in realistic blood flow simulations [24], the use of non-patient-specific flow rate waveforms imposed at the inlet of our models may incorporate some errors. However, this limitation is suffered by most computational studies since flow rate measurements are not routinely acquired in clinical evaluations. This limitation is partially overcome by wall shear stress normalization at inflow segments, which allows comparison between different models. Other model assumptions had limited impact on intra-aneurysmal hemodynamic characterization, as it was shown in a previous work [4].

Conclusions

The present work shows the difference between the intra-aneurysmal hemodynamics before and after the removal of a proximal stenotic plaque. Both idealized and patient-specific models showed significant differences that may impact on the risk of rupture.

Acknowledgements

Marcelo Castro wants to acknowledge CONICET (Consejo Nacional de Investigaciones Científicas y Técnicas) for financial support (PIP CONICET 2011-2013 Nr. 287).

References

[1] Espinosa G, Dzieciuchowicz L, Grochowicz L. Endovascular treatment of carotid stenosis associated with incidental intracranial aneurysm. Ann Vasc Surg 2009:23:688.e1-688.e5

[2] Kappelle LJ, Eliasziw M, Fox AJ, et al. Small unruptured intracranial aneurysm and management of symptatic carotid artery stenosis: North American symptomatic carotid endarterectomy trial group. Neurology 2000:55:307–309

[3] Pappada G, Fiori L, Marina R, et al. Incidence of asymptomatic of asymptomatic berry aneurysms among patients undergoing carotid artery endarterectomy. J Neurosurg Sci 1997:41:257-262
[4] Rouleau, PA, Huston J, Gilbertson J, Brown RD, Meyer FB, Bower TC. Carotid Artery Tandem Lesions: Frequency of Angiographic Detection and Consequences for Endarterectomy. Am J Neuroradiol 2009:20:621-625
[5] Adams HP. Carotid stenosis and coexisting ipsilateral intracranial aneurysm: a problem in management. Arch Neurol 1977:34:515-516
[6] Navaneethan SD, Kanna VS, Osowo A, Shrivastava R, Singh S. Concomitant intracranial aneurysm and carotid artery stenosis: A therapeutic dilemma. Sothern Med J 2006:99(7): 757-758
[7] Cebral JR, Löhner R, Choyke PL, et al. Merging of intersecting triangulations for finite element modelling. J Biomech 2001:34:815–819
[8] Castro MA, Putman CM, Cebral JR. Hemodynamic Patterns of Anterior Communicating Artery Aneurysms: A Possible Association with Rupture. Am J Neuroradiol 2009:30(2):297-302
[9] Cebral JR, Castro MA, Appanaboyina S, Putman C, Millán D, Frangi A. Efficient Pipeline for Image-Based Patient-Specific Analysis of Cerebral Aneurysms Hemodynamics: Technique and Sensitivity. IEEE - Trans Med Imag - Special Issue on Vascular Imaging 2005:24(4): 457-467
[10] Yim PJ, Vasbinder B, Ho VH, et al. A deformable isosurface and vascular applications. Proc SPIE 2002:46841390 –1397
[11] Castro MA, Putman CM, Cebral JR. Patient-specific computational modeling of cerebral aneurysms with multiple avenues of flow from 3D rotational angiography images. Acad Radiol 2006:13:811–821
[12] Löhner R. Automatic unstructured grid generators. Finite Elements Analysis Design 1997:25: 111–134
[13] Löhner R. Extensions and improvements of the advancing front grid generation technique. Comp Meth Appl Mech Eng 1996:5:119–132
[14] Löhner R. Regridding surface triangulations. J Comp Phys 1996:126:1–10
[15] Mazumdar JN. Biofluid Mechanics. World Scientific 1992, Singapore, 41-104
[16] Cebral JR. Castro MA, Putman CM. Alperin, N., Flow-area relationship in internal carotid and vertebral arteries. Physiol Meas 2008:29(10):585-594
[17] Sherman TF. On connecting large vessels to small. The meaning of Murray's law. J Gen Physiol 1981:78:431–453
[18] Womersley JR. Method for the calculation of velocity, rate of flow and viscous drag in arteries when the pressure gradient is known. J Physiol 1955:127:553–563
[19] Taylor CA. Hughes TJR. Zarins CK. Finite element modeling of blood flow in arteries," Comp Meth Appl Mech Engin 1998:158:155–196
[20] Varghese SS, Frankel SH. Fischer PF. Direct numerical simulation of stenotic flows. J Fluid Mech 2007:582:253-280
[21] Varghese SS, Frankel SH. Numerical modelling of pulsatile turbulent flow in stenotic vessels. J Biomech Eng 2003:125:445-460
[22] Patel VC, Rodi W, Scheuerer G. Turbulence models for near-wall and low Reynolds number flows : A review. AIAA J 1984:22:1308-1319
[23] Stroud JS, Berger SA, Saloner D. Numerical analysis of flow through a severely stenotic carotid artery bifurcation. J Biomech Eng 2002:124:9-20
[24] Cebral JR, Pergolizzi RS, Putman CM. Computational fluid dynamics modeling of intracranial aneurysms: Quantitative comparison with cerebral angiography. Acad Radiol 2007:14:804-813